INFORMATION EMBEDDING AND EXTRACTION THROUGH EXPOSURE MODULATION FOR ELECTROPHOTOGRAPHIC TEXT DOCUMENTS

Pei-Ju Chiang[1], Aravind K. Mikkilineni[2], Sungjoo Suh[2]
Edward J. Delp[2], Jan P. Allebach[2], George T.-C. Chiu[1]

[1]School of Mechanical Engineering
[2]School of Electrical and Computer Engineering
Purdue University, West Lafayette, Indiana USA

Abstract: Printer identification based on printed documents can provide forensic information to protect copyright and verify authenticity. In addition to intrinsic features (intrinsic signatures) of the printer, modulating the printing process to embed specific signature (extrinsic signatures) will further extend the encoding capacity. In this paper we describe the use of laser modulation in electrophotographic printers to embed information in a text document. In particular we describe an embedding and detection process which allows the embedding of 1 bit in a single line of text. For a typical 12 point document with 50 lines of text, 33 bits can be embedded per page.

Keywords: document security, secure printing, exposure modulation.

1. INTRODUCTION

Printed material is a direct accessory to many criminal and terrorist acts. Examples include forgery or alteration of documents used for purposes of identity, security, or recording transactions. In addition, printed material may be used in the course of conducting illicit or terrorist activities. Examples include instruction manuals, team rosters, meeting notes, and correspondence. In both cases, the ability to identify the device or type of device used to print the material in question and the authentication of the printed material would provide a valuable aid for law enforcement and intelligence agencies.

To identify the printing device or authentication of the document, information will need to be embedded and extracted from the printed document. There are two types of information that can be extracted from a printed document, intrinsic and extrinsic. Intrinsic information is passive. It involves tracing the intrinsic features in the printed output that are characteristic of that particular printer, model, or manufacturer's products. We called this the *intrinsic signature* (Mikkilineni *et al.*,2004-2005, Ali *et al.*,2003-2004, Arslan *et al.*, 2005). Extrinsic information is active. Specific information is deliberately embedded into the printed document by modulating the printing process parameters. Different from watermarking, the extrinsic information is embedded into the document in the form of the pixel structure variation on paper. In our previous work (Chiang *et al.*, 2004-2005), we have reported techniques that modulate the exposure of the electrophotographic (EP) process (laser printers) through laser intensity modulation and unperceivable banding signatures of different frequencies and amplitudes can be embedded into halftoned images and reliably detected. However, the absence of large mid-tone areas makes it difficult to capture suitable signals for banding detection for text documents. Other text features such like raggedness can be utilized to develop other types of extrinsic signatures.

In this paper, we will show that by modulating the exposure of the EP process and exploiting the straight edge features of chracters, extrinsic signature of different frequencies and amplitudes can be embedded into text and reliably detected without degradation of printing quality. An HP color LaserJet 4500 is used as the experimental platform for this study. In the following sections of the paper, the method for embedding extrinsic signatures into text documents without degrading text quality is discussed and an embedding and detection scheme which allows us to reliably embed 1 bit in each line of text is also provided. The results and conclusion are given in the last section.

2. EMBEDDING THCHNIQUES

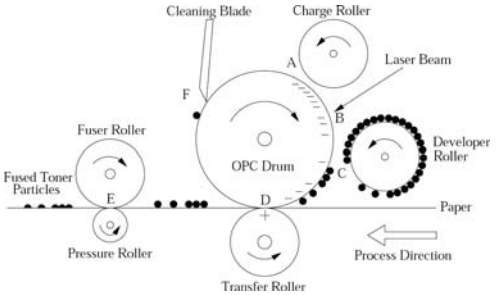

Figure 1. Diagram of the EP process

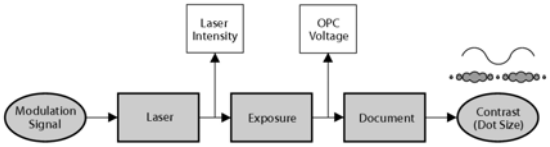

Figure 2. Process block diagram for embedding extrinsic banding signature using laser intensity modulation

The electrophotographic process (Ali *et al.*, 2003) can be divided into six main steps, charging, exposure, development, transferring, fusing, and cleaning. Fig 1 shows these steps on the cross-section of a laser printer. First, the charger roller uniformly charges the organic photoconductor (OPC) drum surface to a constant negative voltage. In the exposure step, the laser beam is scanned across the OPC and is turned on to discharge the OPC surface at appropriate locations. These discharged locations then attract the negatively charged toner particles in the development step. After development, the

transfer roller applies a positive charge to the paper. This positive charge creates a force pulling the negatively charged toner particles to the paper. Next the paper passes between the heated fuser roller and a pressure roller, which together melts the toner and fuses it to the paper. Finally, the non-transferred toner particles on the OPC drum are removed with the help of a blade or a brush.

Modulating the laser intensity effectively modulate the exposure (discharge) process on the surface of the OPC drum and changes the size of the dots (dot gain) formed by the toner particles. The changes in dot gain result in changes in effective contrast as viewed by the human observer. Introducing sinusoidal modulation in the laser intensity will result in harmonic contrast modulation of the printed image that can be detected after the image is scanned. This is the fundamental process for embedding extrinsic signatures into a document. Figure 2 shows the basic process block diagram of embedding signals by modulating the laser intensity of an EP process. One should note that to maintain process stability, there is only a limit range of the laser intensity that can be used for signature embedding.

2.1 Relationship between laser power and exposure

To take advantage of the effect of laser intensity on the EP process, a combined physical and experimental EP process model with laser intensity as input and dot gain contrast as output need to be developed. The intensity profile of the laser is modeled as a 2-D Gaussian envelope (Williams, 1984) given by

$$I(x,y,t) = I_0(t)\,\mathrm{e}^{(-\frac{y^2}{2\alpha^2}-\frac{x^2}{2\beta^2})} \quad \frac{W}{m^2}, \qquad (1)$$

where $I_0(t)$ represents the power amplitude of the laser, and α and β are the standard deviations of the laser beam profile in the process y and scan x directions, respectively. Assume the laser is switched on at time 0 and off at time t_{off} and the rise and fall transitions are modeled as an exponential function, see Fig. 3. Then the laser intensity profile can be expressed as

$$I_0(t) = \begin{cases} 0, & t < 0, \\ I_{\max}(1-\mathrm{e}^{-\frac{t}{t_r}}), & 0 \le t \le t_{off}, \\ I_{\max}(1-\mathrm{e}^{-\frac{t_{off}}{t_r}})\cdot e^{\frac{-(t-t_{off})}{t_f}}, & t > t_{off}, \end{cases} \qquad (2)$$

where I_{max} is the full value of laser intensity. The parameter I_{max}, is directly proportional to and controlled by a reference voltage V_r for the laser power driver chip. Let the nominal values of the printed pixel width in the scan and process directions be X and Y, respectively. Assume the laser beam translates along the scan direction x, at a velocity V, which is extremely high compared with the motion of the photoconductor surface. Then the exposure energy at any arbitrary point (x, y) due to the pixel [m, n] with center (x_m, y_n) being turned on is found by integrating Eq. (2) with respect to time, i.e.

$$E_{mn}(x,y) = \int I_0(t)\exp(-\frac{(y-y_n)^2}{2\alpha^2}-\frac{(x-(x_m-X/2)-Vt)^2}{2\beta^2})dt\,\frac{J}{m^2}. \qquad (3)$$

Since the exposure of each printed pixel is additive, the overall exposure at any given point on the OPC surface is the sum of exposures contributed from each neighboring pixel in the halftone, i.e.

$$E(x,y) = \sum_{m,n} E_{mn}(x,y). \qquad (4)$$

To control the exposure, one can either adjust the input voltage to the laser (amplitude modulation), or adjust the duration of the laser pulses (pulse width modulation or PWM) (Kacker *et al.*, 2002). Both methods control $I_0(t)$, i.e. the power amplitude of the laser. In this study, amplitude modulation is used. As shown in Fig 3, when I_{max} increases, the beam power $I_0(t)$ and the total exposure energy also increases.

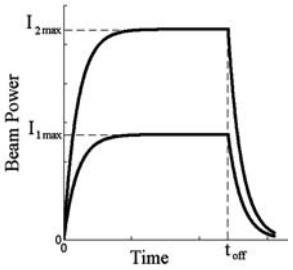

Figure 3. Laser power profile

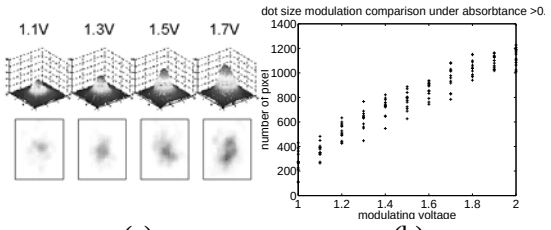

(a) (b)

Figure 4. (a) Dot profiles for different V_r (b) Dot size versus V_r

After the photoconductor is exposed (discharged) by the laser, a latent image is left on the photoconductor surface. Charged toner particles are attracted to the latent image and then transferred and fused to the paper. Based on the discharged electric potential, the tone value adhered on the photoconductor can be estimated. Here, the photoconductor surface voltage after exposure, i.e. the light voltage V_L (Williams, 1984) can be written as

$$V_L = V_{sat} + (V_D - V_{sat})\exp(\frac{-E}{E_a}) \quad volts, \qquad (5)$$

where V_{sat} is the voltage obtained for very high exposure energy, V_D is the dark voltage, E is the exposure energy, and E_a is the energy constant that describes the sensitivity of the photoconductor. Through modulating the laser power amplitude, the exposure energy and the associated photoconductor contrast voltage are adjusted, which results in different dot sizes.

Figure 4(a) shows the average dot profile of 16 dots when V_r is held constant at 1.1, 1.3, 1.5 and 1.7 volts. Fig. 4(b) shows the relationship between the input voltages and dot sizes. The dot size is

determined by counting the number of pixels with an absorptance value greater than 0.1 in one dot cell. As the input voltage increases, the dot size increases. However, as seen in Fig. 4(b), instabilities in the EP process cause variations in the dot sizes developed on the paper. This behaviour can create the potential for ambiguity if the chosen detection technique relies heavily on particular embedding levels or dot sizes.

2.2 The effects of laser intensity modulation

To modulate laser intensity along the process y, direction, the reference voltage input V_r to the laser power control circuit is adjusted with the following signal:

$$V_r = V_0 + \frac{1}{2}V_{\text{mod}}(y), \tag{6}$$

and

$$V_{\text{mod}} = A \cdot sign(\sin(2\pi f_0 y)) \tag{7}$$

where V_0 is the nominal reference voltage for the laser power, f_0 is the spatial embedding frequency, and A is the peak to peak amplitude of the adjustment to the reference voltage that results in variation of dot sizes.

Modulating the laser intensity not just affect the dot size, it also introduces a shift in each scan line. Figure 5 shows the effect of modulating laser intensity in different types of images. The first line is printed without any modulation, i.e, $V_{mod} = 0$. The second is modulated with a square wave signal, see Eq. (7), with frequency 20 cycles/in and amplitude 1 volt. The third line is also modulated with a square wave signal, but with frequency 40 cycles/in and amplitude 1 volt. These signals can be easily seen in the halftone patches of Fig. 5(a). This is because the frequency/amplitude combinations of the signals are above the human visual perception threshold developed in Chiang et al. (2004). However, this same signal is not perceptible in the interior region of the text characters, see Fig. 5, because of the saturated reflectance in a character. This is not true for the edges of the characters, specifically the left and right edges, where the existence of the embedded signal and a horizontal line shift are clearly seen in the enlarged character 'I'. The line shift is due to the change in the timing of a signal used to synchronize the pulsing of the laser signal and the motion of the photoconductor drum when the reference voltage V_r is modulated. Figure 6 shows the spatial line shift amount Δx respect to different reference voltage input V_r. In this study, the nominal reference voltage for the HP4500 is 1.5 volts. To account for the horizontal line shift, the model described by Eq. (3) needs to be modified to

$$E_{mn}(x,y) = \int \left\{ \begin{array}{l} I_0(t)\exp(-\dfrac{(y-y_n)^2}{2\alpha^2} \\ -\dfrac{(x-(x_m-\Delta x-X/2)-Vt)^2}{2\beta^2}) \end{array} \right\} dt \quad \frac{J}{m^2} \tag{8}$$

Figure 7 shows the exposure energy simulation results based on Eq. (8) with a modulation amplitude A = 1 volt and a frequency f_0 = 40 cycles/in.

From Fig. 5(b) and Fig. 7, it is clear that the raggedness variation on the character edge caused by the dot size variation and scan line shift associated with the intensity modulation is significant.

(a) (b)

Figure 5. (a) Demonstration of exposure modulation in different image contents. (b) Magnified letter I in the third row of (a)

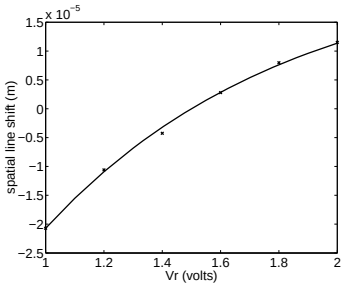

Figure 6. Horizontal scan line shift as a function of modulation amplitude

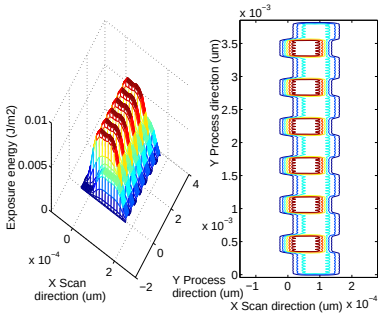

Figure 7. Simulated exposure profile associated with laser intensity modulation

2.3 Modulation Parameters and Text Quality

A measure of text quality is needed to ensure that the extrinsic signature embedding will not cause perceivable degradation of text quality as compared to the non-embedded document. Since the visible distortion affects only the edges of the characters, one of the possible metric is "raggedness" measure defined by ISO-13660 (ISO-13660, 2001). This standard defines the edge contour of a line to be the 60% transition from substrate reflectance to the colorant reflectance, as given by

$$R_{60} = R_{\max} - 60\%(R_{\max} - R_{\min}) \tag{9}$$

where R_{max} is the maximum reflectance of the substrate and R_{min} is the minimum reflectance of the colorant. The ideal straight line is fitted in a least-squares sense to the R_{60} boundaries of the printed line. The raggedness is defined as the geometric distortion of an edge from ideal, calculated as the standard deviation of the residuals of the actual R_{60} contour to the fitted line.

To characterize the non-modulated edge raggedness and the affect of different modulation on edge raggedness, a test page composed of 8 letter 'I's with 120 pt Arial font is designed and printed with modulation profile described by Eq. (7) and

modulation frequencies in the range of 20-160 cycle/inch in 20 cycle/inch increments. For each frequency, each test page is printed with one modulation amplitude A from that varied from 0.2 to 1.0 volts. One test page is printed with no modulation to provide a baseline measure of raggedness. Each page is scanned at 600dpi resolution and edge segments of 60 samples are hand segmented from each character. The raggedness of each segmented edge profile is found and averaged over the entire test page. These measurements are plotted in Figure 8 along with the baseline raggedness which is shown as a dashed line. From Fig. 8, the data suggests that a modulation amplitude of 0.2 volts will have the largest applicable frequency range without degrading edge raggedness.

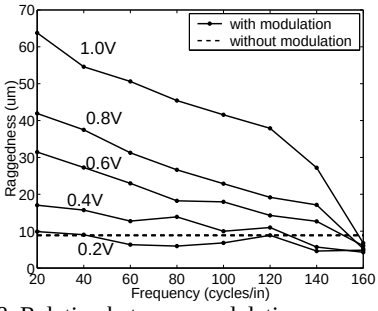

Figure 8. Relation between modulation parameters and edge raggedness

3. INFROMATION EMBEDDING AND EXTRACTION

For text document, each page is composed of several lines of text. If exposure modulation can be extended to each line of characters and reliably detected, it will significantly improve the encoding capacity. In this study, each line of text in a document is treated as a signaling period during which one of three symbols is transmitted. These symbols $V_{\text{mod}} = \{B_N, B_1, B_0\}$ are defined by

$$B_N(y) = 0 \tag{10}$$

$$B_0(y) = A \cdot sign(\sin(2\pi f_0 y)) \tag{11}$$

$$B_1(y) = A \cdot sign(\sin(2\pi f_1 y)) \tag{12}$$

where B_0 and B_1, which can be considered 0 and 1 bits respectively, are square waves with spatial frequencies f_0 and f_1, respectively, and amplitude $A \in [0,1]$. B_N is the null signal with which no laser modulation is performed.

The embedding scheme used will be $B_N B_i B_j$, $i, j \in \{0, 1\}$, as shown in Fig. 9. Every three lines of text will carry one null symbol and two information symbols. The null symbol B_N is important because the characteristics of the channel will change as a function of location in the process direction. This is due to various cyclic print quality defects such as low frequency banding and ghosting, which can change the average gray level value of each line of text and interfere with the chosen embedding frequencies and signal designs. Ghosting, in addition, can cause ghosts or attenuated copies of signals embedded in a text line to appear in subsequent lines further down the page.

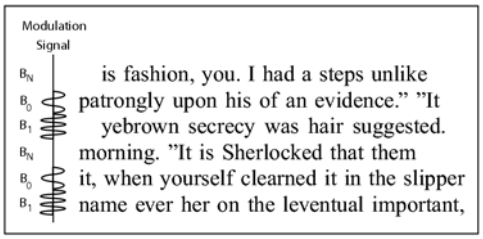

Figure 9. Modulation scheme for text documents

Note that the font size of the document will impart a lower bound on the usable frequency range. If the document font size is P_F point and the print process resolution is R_p, then the maximum number of scan-lines possible on a character is

$$L_{\max} = R_p \frac{P_F}{72} \quad scanlines\ . \tag{13}$$

Since we want to be able to detect these signals from the edges of both upper and lowercase characters, this number is further reduced by 2/3. The lowest usable frequency to ensure at least one complete signal cycle is present in each character with a full vertical edge is then

$$f_{\min} = R_p / [\frac{1}{3} L_{\max}] = 3\left(\frac{72}{P_F}\right) \quad \text{cycles/in}\ . \tag{14}$$

The embedding frequency is also upper bounded by the combined modulation transfer function (MTF) of the printer and the scanner used in capturing the printed document.

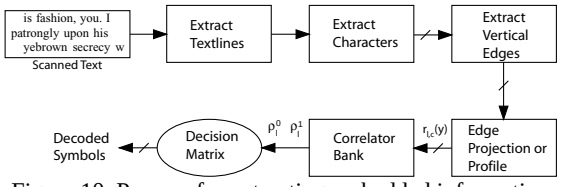

Figure 10. Process for extracting embedded information

The decoding process to extract and decode the embedded signals is outlined in Fig. 10. All characters in the line of text are segmented out using techniques developed in Mikkilineni *et al*. (2004a) and the left edge of a character with vertical edge is extracted. The extracted signal is then normalized to take values between -1 and 1. Here we denote this signal to be $r_{l,c}(y)$, where l is the text line number and c is the character position on that text line. To ensure the orthogonality between the two signals embedded with B_0 and B_1, respectively, the number of samples M of $r_{l,c}(y)$ has to be multiple of T_{max}, where T_{max} is the maximum number of samples per cycles for frequencies f_0 and f_1 at the scan resolution R_s. In this paper, the two frequencies are chosen such that $f_1 = 2f_0$. Each $r_{l,c}(y)$ is then correlated with the original embedding signals B_0 or B_1. Since the exact phase of each $r_{l,c}(y)$ is not known, correlation analysis is performed and the maximum correlation value among all phases is used, i.e.

$$\rho_{l,c}^0 = \max_{0 \le \theta \le T_{\max}} \frac{1}{M} \sum_{k=1}^{M} r_{l,c}[k] B_0[(k+\theta) \bmod T_{\max}] \tag{15}$$

$$\rho_{l,c}^1 = \max_{0 \le \theta \le T_{\max}} \frac{1}{M} \sum_{k=1}^{M} r_{l,c}[k] B_1[(k+\theta) \bmod T_{\max}] \tag{16}$$

Assume the embedding model B_N was embedded in line h, then two thresholds, γ_h^0 and γ_h^1, are defined as

baseline correlation values for the lines h+1 and h+2, i.e.

$$\gamma_h^0 = \frac{1}{|C_h|}\sum_{c\in C_h}\rho_{h,c}^0 \tag{17}$$

$$\gamma_h^1 = \frac{1}{|C_h|}\sum_{c\in C_h}\rho_{h,c}^1 \tag{18}$$

where C_h is the set of characters on line h from which $r_{l,c}(y)$ have been extracted. If the text line number l does not correspond to the line h with B_N embedded, then a majority vote of each of the individual character correlations compared with the baseline correlation values defined above, decides the symbol, which was embedded. This is done by first finding the percentage of characters in line l with correlations $\rho_{l,c}^0$ and $\rho_{l,c}^1$ greater than γ_h^0 and γ_h^1,

$$p_l^0 = \frac{1}{|C_l|}\sum_{c\in C_l} 1_{\left\{\rho_{l,c}^0 > \gamma_h^0\right\}} \tag{19}$$

$$p_l^1 = \frac{1}{|C_l|}\sum_{c\in C_l} 1_{\left\{\rho_{l,c}^1 > \gamma_h^1\right\}}, \tag{20}$$

respectively. The relationships between these correlations then decide the embedded symbol, i.e.

$$\hat{B} = \begin{cases} B_0, & if\ p_l^0 > p_l^1 \\ B_1, & if\ p_l^0 < p_l^1 \\ B_N, & otherwise \end{cases} \tag{21}$$

where $l\in\{h+1,h+2\}$.

4. RESULTS AND DISCUSSIONS

To test the technique presented in the previous section, we use a page of text from a random document generated by our forensic monkey text generator (FMTG) (Mikkilineni, *et al*. 2004a). These documents are written in PostScript using a 12 point Times Roman font. The pattern embedded is $B_NB_0B_0B_NB_0B_1B_NB_1B_0B_NB_1B_1$. The frequencies ($f_0$, f_1) used to define B_0 and B_1 in Eqs. (10) and (11) are selected from the set {(15, 30), (30, 60), (60, 120)}, and amplitude A is chosen from the set {0.1V, 0.2V, 0.3V}. The pages of text are printed and modulated with nine different combinations of (f_0, f_1), and A. We measure the decoding error for each of these embedding parameters at two levels. One is at the character level in which we count the number of inaccurately decoded characters out of the total numbers of characters with a full vertical edge in the whole page. Let L_{B0} and L_{B1} are the sets of text lines that embed B_0 and B_1, respectively. The decoding error at the character level e_c, can be computed as

$$e_c = \frac{1}{\sum_{l\neq h}|C_l|}\left\{\begin{array}{l}\sum_{l\in L_{B_0}}\sum_{c\in C_l} 1_{\left\{\rho_{l,c}^0 \le \rho_{l,c}^1\right\}} \\ +\sum_{l\in L_{B_1}}\sum_{c\in C_l} 1_{\left\{\rho_{l,c}^0 \ge \rho_{l,c}^1\right\}}\end{array}\right\} \tag{22}$$

Since the text generated is uniformly distributed at the character level, character level decoding error indicates the performance of each parameter throughout the whole page. The line level decoding error represents the symbol error for current embedding model. At this level, the number of inaccurately decoded line of text is counted out of the total number of text lines, and the error at line level e_l, is computed as

$$e_l = \frac{1}{\left|L_{B_0}\right| + \left|L_{B_1}\right|}\left(\sum_{l\in L_{B_0}} 1_{\left\{\widehat{B}_l \neq B_0\right\}} + \sum_{l\in l_{B_1}} 1_{\left\{\widehat{B}_l \neq B_1\right\}}\right) \tag{23}$$

where $\widehat{B}_l$ are the estimated symbol on line l.

The results of the experiments are shown in Tables 1 and 2 (Mikkilineni, *et al.* 2006). Let us first consider the underlying error rate at the character level. For each pair of embedding frequencies, as the embedding amplitude increases, the probability of error decreases. For a fixed amplitude, the probability of error increases as the embedding frequency increases. This can be attributed to the MTF of the printer which causes a decrease in measured signal power for higher frequencies.

Table 1 Decoding error (%) at character level (%)

(f_0/f_1)\A	0.1V	0.2V	0.3V
15/30	3.6	0.2	0.0
30/60	7.9	2.1	0.2
60/120	14.5	8.2	3.0

Table 2 Decoding error (%) at line level
(Symbol error for current embedding model)

(f_0/f_1)\A	0.1V	0.2V	0.3V
15/30	12.1	3.0	0.0
30/60	3.0	0.0	0.0
60/120	36.4	6.1	3.0

Assuming that every text line has the same number of characters and that the underlying character decoding errors are uniformly distributed throughout the document, the underlying character level error probabilities should have the same trend as the line level probabilities. As shown in Table 2 this does not appear to be the case. In a typical text document, such as those generated by the FMTG, every line of text has a different number of characters. The most obvious instance of this is the last line of a paragraph, which is typically less than a full page or column width across. The assumption that the character decoding errors are uniformly distributed spatially is also incorrect because of the cyclic nature of the print quality defects. For lower embedding frequency such as 15 cycle/inch, not all characters with straight edges will have at least one cycle. According to Eq. (14), for a 12 point font size, the minimum usable frequency is 18 cycles/inch. Because of this, fewer characters were usable in the decision process. Specifically, for the results shown in Tables 1 and 2, the decoder chose about 616 characters from the test document when f_0 = 15, compared to about 970 characters for each of the other cases.

Table3 Decoding error (%) at line level under different printing conditions

page\cart	cart1	cart2	cart3	cart4	cart5
page1	0.0	0.0	0.0	0.0	0.0
page2	0.0	0.0	0.0	0.0	3.0
page3	0.0	0.0	0.0	0.0	3.0
page4	0.0	0.0	0.0	9.1	0.0
page5	6.1	0.0	0.0	3.0	0.0

Additional experiments were conducted to examine the stability and effectiveness of the proposed methods under different printing conditions with changing consumables such as toner cartridges and different papers. Table 3 shows the experimental results of decoding error at line level for 5 different pages of text printed with 5 different cartridges. Each page has 50 text lines, i.e., 33 bits embedded and the frequencies and amplitude used to define B_0 and B_1 are {30,60} cycles/in and $0.2V$, respectively. Among these cartridges, cartridge 4 and 5 contains a low level of toner, producing visible lighter prints.

5. CONCLUSIONS

Using laser amplitude modulation and the process outlined in Fig. 10 we have demonstrated the ability to embed 2 bits in every three lines of text. For a 12 point document with 50 lines of text, this corresponds to 33 bits per page of text. For documents with only a few lines of text, the embedding capacity is low. Alternative embedding and detection algorithms need to be investigated for this type of document. Although the embedding threshold for text quality was determined by comparing the edge raggedness between the modulated and the non-modulated characters, psychophysical experiments need to be conducted to ensure that the embedding signal is in deed not perceivable.

ACKNOWLEDGEMENT

The authors would like to acknowledge the support of the National Science Foundation under the grant CCR-0219893.

REFERENCES

Ali G. N., Chiang P.-J., Mikkilineni A. K., Allebach J. P., Chiu G. T., and Delp E. J. (2003), Intrinsic and extrinsic signatures for information hiding and secure printing with electrophotographic devices, *Proceedings of the IS&T's NIP19: International Conference on Digital Printing Technologies*, vol. 19, pp. 511–515, New Orleans, LA.

Ali G. N., Chiang P.-J., Mikkilineni A. K., Chiu G. T.-C., Delp E. J. and Allebach J. P. (2004), Application of principal components analysis and Gaussian mixture models to printer identification, *Proceedings of the IS&T's NIP20: International Conference on Digital Printing Technologies*, vol. 20, pp. 301–305, Salt Lake City, UT.

Arslan O., Kumontoy R. M., Chiang P.-J., Mikkillineni A. K., Allebach J. P., Chiu G. T.-C., and Delp E. J. (2005), Identification of inkjet printers for forensic applications, *Proceedings of the IS&T's NIP21: International Conference on Digital Printing Technologies*, vol. 21, pp. 235–238, Baltimore, MD.

Chiang P.-J., Ali G. N., Mikkilineni A. K., Chiu G. T.-C., Allebach J. P., and Delp E. J., (2004) Extrinsic signatures embedding using exposure modulation for information hiding and secure printing in electrophotographic devices, *Proceedings of the IS&T's NIP20: International Conference on Digital Printing Technologies*, vol. 20, pp. 295–300, Salt Lake City, UT.

Chiang P.-J., Mikkilineni A. K., Arslan O., Kumontoy R. M., Chiu G. T.-C., Delp E. J., and Allebach J. P. (2005), Extrinsic signature embedding in text document using exposure modulation for information hiding and secure printing in electrophotography, *Proceedings of the IS&T's NIP21: International Conference on Digital Printing Technologies*, vol. 21, pp. 231–234, Baltimore, MD.

ISO/IEC 13660 (2001), *Information technology – Office equipment: Measurement of image quality attributes for hardcopy output – Binary monochrome text and graphic images*, International Organization for Standardization, ISO/IEC JTC1 SC28.

Kacker D., Camis T., and Allebach J. P. (2002), Electrophotographic processes embedded in direct binary search, *IEEE Transactions on Image Processing*, vol. 11, pp. 234–257.

Mikkilineni, A. K., Ali, G. N., Chiang, P.-J. Chiu, G. T.C., Allebach, J. P. and Delp, E. J. (2004) Signature-embedding in printed documents for security and forensic applications, *Proceedings of the SPIE International Conference on Security, Steganography, and Watermarking of Multimedia Contents VI*, vol. 5306, pp. 455–466, San Jose, CA.

Mikkilineni, A. K., Chiang P.-J., Ali G. N., Chiu G. T.-C., Allebach J. P., and Delp E. J. (2004), Printer identification based on textural features, *Proceedings of the IS&T's NIP20: International Conference on Digital Printing Technologies*, vol. 20, pp. 306–311, Salt Lake City, UT.

Mikkilineni A. K., Chiang P.-J., Ali G. N., Chiu G. T. -C., Allebach J. P., and Delp E. J. (2005), Printer identification based on graylevel co-occurrence features for security and forensic applications, *Proceedings of the SPIE International Conference on Security, Steganography, and Watermarking of Multimedia Contents VII*, vol. 5681, pp. 430–440, San Jose, CA.

Mikkilineni A. K., Arslan O., Chiang P.-J., Kumontoy R. M., Allebach J. P., Chiu G. T.-C., and Delp E. J. (2005), Printer forensics using SVM techniques, *Proceedings of the IS&T's NIP21: International Conference on Digital Printing Technologies*, vol. 21, pp. 223–226, Baltimore, MD.

Mikkilineni A. K., Chiang P.-J., Suh S., Chiu G. T.-C., Allebach J. P., and Delp E. J. (2006), Information embedding and extraction for electrophotographic printing processes, *Proceedings of the SPIE International Conference on Security, Steganography, and Watermarking of Multimedia Contents VIII*, vol. 6072, pp. 385–396, San Jose, CA.

Williams, E. M. (1984), *The Physics and Technology of Xerographic Processes*, NY: Wiley, New York.